In Situ SAXS Analysis of Silica Gel Formation with an Additive

Cédric Gommes,*,† Silvia Blacher,† Bart Goderis,‡ René Pirard,† Benoît Heinrichs,† Christelle Alié,† and Jean-Paul Pirard†

Laboratoire de Génie Chimique, Département de Chimie Appliquée, Université de Liège, bâtiment B6a, B4000 Liège, Belgium, and Laboratorium voor Macromoleculaire Structuurchemie, Departement Scheikunde, Katholieke Universiteit Leuven,Celestijnenlaan 200F, B3001 Heverlee, Belgium

Received: January 30, 2004; In Final Form: April 24, 2004

Time-resolved small-angle X-ray scattering (SAXS) measurements performed during the formation of tetraethyl orthosilicate (TEOS) based silica gels in alcohol with 3-(2-aminoethylamino)propyltrimethoxysilane (EDAS) as an additive are reported. The measurements reveal no discontinuity of the nanostructure at the gel point. A chemically induced spinodal phase separation is found to give a coherent picture of the collected data. Increasing the amount of EDAS induces the phase separation on a smaller length scale, which finally leads to a modified gel morphology. The SAXS measurements and the electron micrographs associated with the dry gels could be interpreted in terms of the suggested wet gel formation mechanism.

1. Introduction

The preparation of porous solids by sol−gel processes consists of synthesizing a gel from an organic solution followed by the removal of the solvent in order to obtain a dry material. Thanks to their high versatility, sol−gel methods are widely used to produce materials with specific properties.[1] In particular, silica aerogels have been found to be useful in several applications, such as low-temperature synthesis of glasses, as insulating materials,[2] and in many other applications related to their extraordinarily high porosity.[3]

To characterize the texture of the finally obtained materials, vapor adsorption, mercury porosimetry, and electron microscopy are often used. The synthesis parameters that are thought to have the deeper impact on the final material concern the chemical reaction in the gelling solution. Therefore, to control the texture of the final material, it is useful to study in situ how the gel is formed. To achieve this, scattering techniques are powerful since they allow a noninvasive characterization of the material morphology at the nanometric scale. This methodology was applied by several authors to investigate how inorganic polymer systems, such as SiO_2,[4−6] TiO_2,[7] and ZrO_2[8,9] gels, are formed. In the general mechanism that follows from these studies, the materials are obtained via the formation of elementary building blocks that, in a secondary stage, aggregate until the resulting clusters fill the space. The large variety in structures results from differences in the details of the building blocks and in their aggregation mechanism, which are governed by the nature of the precursor and by the synthesis conditions.[1] Small-angle X-ray scattering (SAXS) patterns of these materials consists of a continuously decreasing intensity with increasing scattering angle—without any maximum—and is often interpreted in terms of fractal geometry.[10] This also holds for the dry materials, obtained after solvent removal, that usually have a highly hierarchical nanostructure, with a large porosity and high specific surface.

On the other hand, a phase separation mechanism has been proposed for the formation of resorcinol/formaldehyde organic porous materials obtained by a sol−gel process, and with textural properties similar to the mentioned inorganic porous materials.[11,12] Such phase separation phenomena are often invoked to describe the texture of as-synthesized organic polymer materials.[14−16] Visible light scattering measurements[17] or SAXS[18] performed on these structures usually gives rise to a peak which is reminiscent of a characteristic length in the system.

The present paper analyzes in situ SAXS data collected during the formation of SiO_2 gels obtained by adding 3-(2-aminoethylamino)propyltrimethoxysilane (EDAS) in various proportions to a tetraethylorthosilicate (TEOS) based alcoholic solution, and dried in subcritical conditions. The use of this particular additive guarantees a large porosity, even when the gels are dried in subcritical conditions, which makes them useful as catalyst supports.[19] The chemical reactions involved in the gel formation are hydrolysis and condensation. The hydrolysis of TEOS can be written as

$$(OC_2H_5)_4Si + nH_2O \rightarrow (OC_2H_5)_{4-n}(OH)_nSi + nC_2H_5OH \quad (1)$$

where n can take any value from 1 to 4. Similarly, the hydrolysis of EDAS obeys

$$(OCH_3)_3SiR + nH_2O \rightarrow (OCH_3)_{3-n}(OH)_nSiR + nCH_3OH \quad (2)$$

where n can take any value from 1 to 3, and R is the following nonhydrolyzable organic group:

$$R = -(CH_2)_3NH(CH_2)_2NH_2 \quad (3)$$

Two partially hydrolyzed molecules can link together by either of the following condensation reactions

$$\cdots SiOH + HOSi\cdots \rightarrow \cdots SiOSi\cdots + H_2O$$

$$\cdots SiOR' + HOSi\cdots \rightarrow \cdots SiOSi\cdots + R'OH \quad (4)$$

* Corresponding author. Telephone: +32 (0)4 366 29 51. Fax: +32 (0)4 366 35 45. E-mail: Cedric.Gommes@ulg.ac.be.
† Université de Liège.
‡ Katholieke Universiteit Leuven.

10.1021/jp049568a CCC: $27.50
Published on Web 05/29/2004

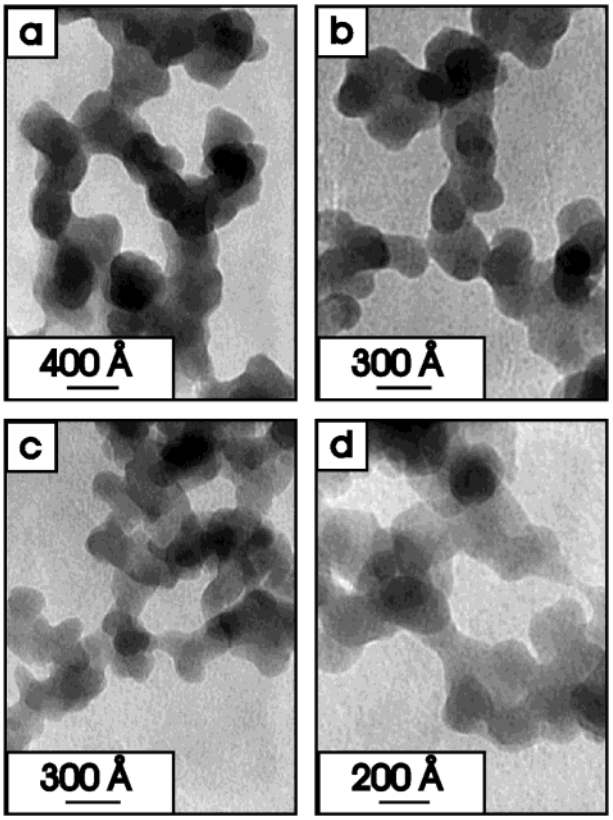

Figure 1. Example of TEM micrographs obtained from fragments of dry gels synthesized with various EDAS/TEOS ratios. EDAS/TEOS = 0.025 (a), 0.04 (b), 0.06 (c), and 0.2 (d).

where, in the second reaction, R′ can be either a methyl or ethyl group according to whether the condensation concerns a TEOS-derived or an EDAS-derived molecule.

Nitrogen adsorption, mercury porosimetry, and electron microscopy all show that the texture of the obtained dry material depends on the amount of EDAS used during the synthesis.[20,21] The transmission electron micrographs in Figure 1 illustrate the typical appearance of dry gel fragments obtained for various amounts of EDAS. The nanometric structure can be thought of as made of elongated aggregates of globular silica particles and is sometimes described as a string of pearls.[11,12] The size of these objects decreases when the EDAS/TEOS ratio is increased.

Although some mechanisms have been proposed,[20] at the present stage it is unknown how EDAS controls the texture of the synthesized materials at the nanometric scale. In particular, the question has to be answered whether EDAS acts as a drying control chemical agent[22] or whether it plays a major role during the formation of the wet gel. To gain a deeper insight into these issues, time-resolved SAXS measurements were performed on the gelling solutions and the dry materials were investigated by static SAXS, for various amounts of EDAS. The results are critically analyzed in the light of existing phase separation and aggregation models.

2. Experimental Section

2.1. Synthesis of the Samples. Gels are made from tetraethyl orthosilicate (TEOS), 3-(2-aminoethylamino)propyltrimethoxysilane (EDAS), H_2O, ethanol, and NH_4OH via a single-step base-catalyzed hydrolysis and condensation. To a mixture containing EDAS, TEOS, and half the ethanol, a solution of aqueous NH_3 in the remaining ethanol is added under stirring. The stirring is then stopped and the flask is closed. The water solution has an NH_3 content of 0.18 mol/L. The hydrolysis ratio $H = H_2O/(TEOS + (3/4)EDAS)$ is kept at the value of 4. The 3/4 factor is justified by the fact that EDAS only contains 3 hydrolyzable groups, while TEOS contains 4 of them. A dilution ratio R = ethanol/(TEOS + EDAS) of 10 is chosen for all samples. Four solutions with EDAS/TEOS ratios = 0.025, 0.04, 0.06, and 0.2, respectively, are studied and referred to hereafter as ET025, ET04, ET06, and ET2. These particular EDAS/TEOS values were chosen on the basis of a previous work as giving rise to regularly spaced silica nanoparticle sizes.[20]

To obtain the final dry material, the gels are aged at 60 °C for 7 days. Next, the flasks are opened and put into a drying oven heated to 60 °C where, over a period of 1 week, the pressure is progressively lowered from atmospheric to 12 mbar and the temperature is raised to 150 °C.

2.2. SAXS Measurements. Small-angle X-ray scattering (SAXS) measurements were performed at DUBBLE, the Dutch−Flemish CR6 beam line (BM26B) at the European Synchrotron Radiation Facility (ESRF) in Grenoble, France. Promptly after adding the water/ethanol mixture to the TEOS/EDAS/ethanol solution and stirring, a small sample is extracted from the flask and placed in a 1.5 mm thick cell with parallel mica windows. The gel point of the solution is determined off line in the synthesis flask. Consecutive in situ pinhole SAXS patterns are recorded over time spans of 10 s on a quadrant detector placed at 4.25 m from the sample. Corrections were made for the detector response, and the data were normalized to the intensity of the primary beam measured by an ionization chamber placed upstream from the sample. The SAXS intensity is expressed as a function of the scattering vector modulus, q, which was calibrated using a collagen standard and with $q = (4\pi/\lambda)\sin(\theta/2)$, λ being the wavelength (1 Å) and θ the scattering angle. The normalized intensity scattered by the empty sample holder was measured and subtracted from the scattering patterns.

3. Results

3.1. Time-Resolved SAXS Measurements of the Gelling Solutions. Figure 2 shows the scattering patterns, $I(q,t)$, as a function of the scattering vector, q, and the time, t, using linear scales. For all samples, a peak appears early during the reaction. Its intensity progressively increases and its position shifts toward smaller scattering angles with time, as emphasized in each pattern by the circles. The thick black line corresponds to the gel time, which is when the solution left in the synthesis flask no longer flows when it is tilted. One observes from the patterns that the gel point does not coincide with any particular event occurring at the length scales explored by the SAXS. At very low angles ($q < 0.01$ Å^{-1}), the scattered intensity seems to increase with decreasing q, which suggests the existence of larger structures that are inaccessible with the used experimental setup. The gel structural evolution on a nanometric scale of all samples seems to level off toward the end of the experiment except for ET2.

The peak is a characteristic of the low-q part of the scattering patterns. As far as the high-q regions are concerned, they are often analyzed by viewing them on a double logarithmic plot as in Figure 3. Since the evolution in ET2 seems not to be ended after 3 h, the same cell was measured again another 3 h later, i.e., 6 h after the beginning of the reaction, and the corresponding pattern is also plotted in Figure 3d. Apparently an asymptotic power law at high q exists toward the end of the experiment. At shorter times no linear region can be identified.

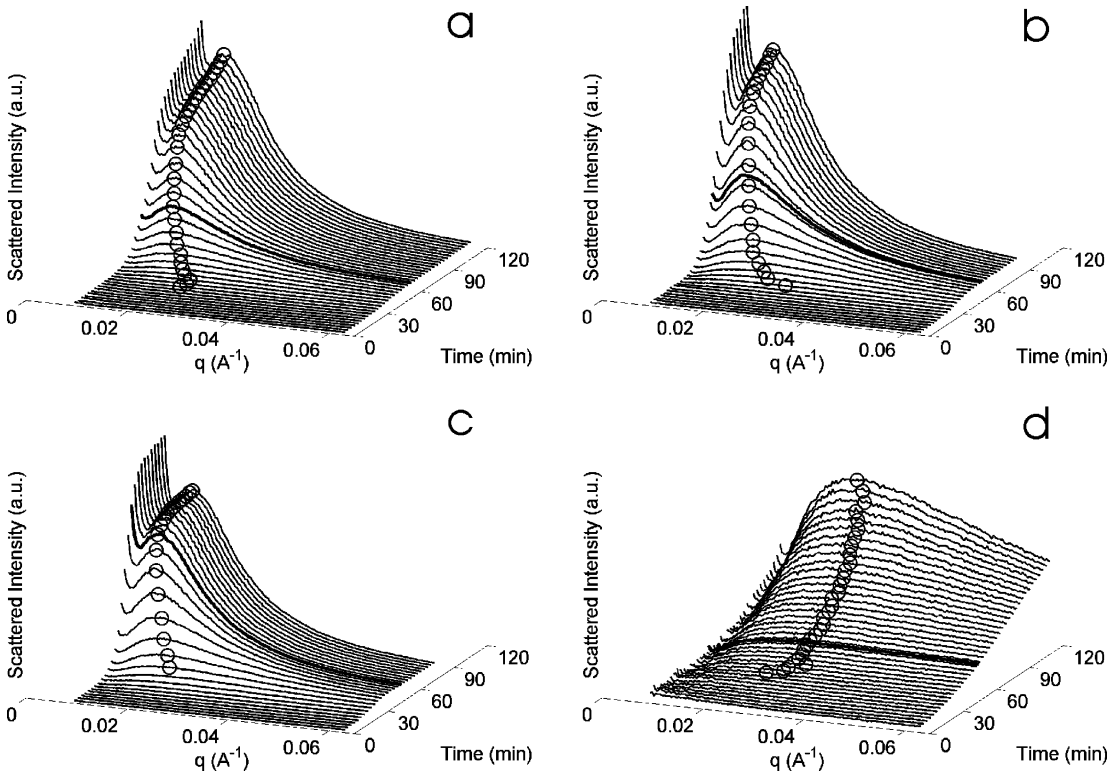

Figure 2. Time-resolved SAXS measurements performed on gelling solutions for samples ET025 (a), ET04 (b), ET06 (c), and ET2 (d). For the sake of clarity, the maximum of the peak is highlighted with a circle when it is visible. The thick solid line is the spectrum corresponding to the gel point, as assessed by the fact that the solution no longer flows when the vessel is tilted.

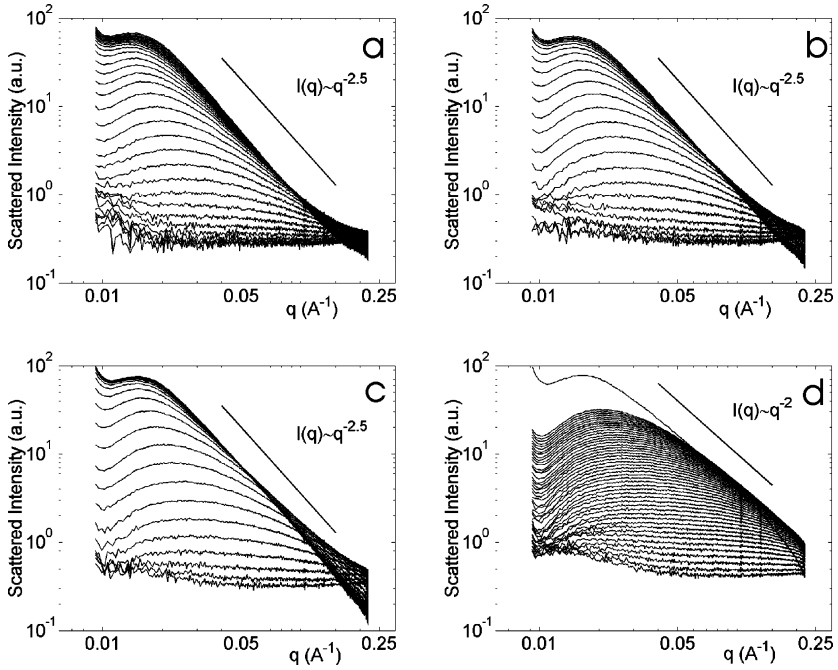

Figure 3. Logarithmic representations of the time-resolved SAXS measurements of the gelling solutions for samples ET025 (a), ET04 (b), ET06 (c), and ET2 (d). On each graph the curves are separated by 1.5 min. For sample ET2 the pattern recorded on the 6-hour-old gel is represented.

The total scattered intensity, the so-called invariant Q,[23,24] is defined as

$$Q = \int_0^\infty q^2 I(q)\, \mathrm{d}q \qquad (5)$$

Since the scattering pattern is only measured on a limited q interval, this quantity can only be estimated approximately. For scattering patterns exhibiting a clear Porod behavior, the intensity is usually extrapolated outside of the measured q range in order to calculate Q. In the present case, a -4 asymptotic exponent is not observed (Figure 3). Therefore, such an extrapolation would amount to making a hypothesis on the structure of the system at smaller scales than actually observed. In order not to bias the analysis by making an a priori assumption on the structure of the system, Q was here estimated from eq 5 by limiting the integration to the measured q range. Since this might result in a significant error in the estimation of Q, the evolution of this parameter will be only discussed

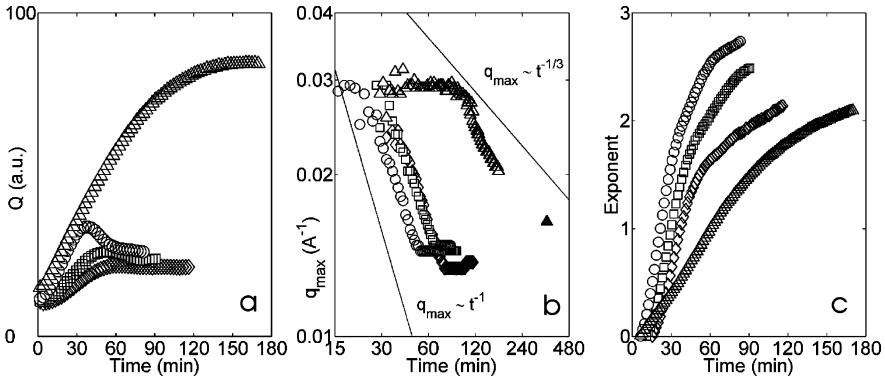

Figure 4. Time evolution of the invariant Q (a), of the q-position of the peak (b), and of the indicative asymptotic exponent in the high-q range (c), for samples ET025 (◇), ET04 (□), ET06 (○), and ET2 (△). Note the logarithmic scales for part b.

qualitatively. For ET025, ET04, and ET06 an oscillation is visible in the Q vs time curves (Figure 4a), whose amplitudes increase with the EDAS/TEOS ratio. In the case of ET2 the evolution of Q seems to be monotonic. For the sake of completeness, the invariant was also estimated by extrapolating the data with a Porod law (not shown) and the same trends are observed.

Figure 4b displays on logarithmic axes the time evolution of the position of the peaks' maximum. The extra ET2 point in this figure is associated with the 6-hour-old gel. For every sample there exists a time interval in which the evolution obeys a power law. Two specific theoretical power laws are added to this particular figure and contribute to the Discussion section.

Although an asymptotic linear trend is not visible at early times in Figure 3, a slope was extracted anyway (Figure 4c), serving to characterize the shape evolution of the scattering patterns. The characteristic exponents that can be read from the slopes of the curves increase continuously with time, and at the end of the runs their values lie between -2 and -3 for all samples.

The SAXS patterns were also analyzed by fitting with a theoretical model that is compatible with the prevailing ideas on sol−gel transitions, i.e., the aggregation of particles. Its mathematical expression is

$$I(q) = S(q)\,P(q) \tag{6}$$

where $P(q)$ is the form factor describing both the size and shape of the particles and $S(q)$ is a structure factor reflecting their interactions.[23−25] In this equation, the shape of the function $P(q)$ affects the high-q region of the SAXS patterns, whereas $S(q)$ is significantly different from 1 only in the low-q region.

The choice of a particular functional form of $P(q)$ should be based on the high-q behavior of the scattered intensity. Figure 3 shows that toward the end of the runs the patterns exhibit a power law decay in this region. Therefore, the following fractal-like function was used as a form factor:[26]

$$P(q) = P_0\left(1 + \frac{1}{(qr_0)^D}\frac{D\Gamma(D-1)}{[1+1/(q\xi)^2]^{(D-1)/2}}\sin[(D-1)\tan^{-1}(q\xi)]\right) \tag{7}$$

where Γ is the gamma function, ξ is a correlation length that can be thought of as the size of the fractal particles, D is their fractal dimension, r_0 is the radius of the elementary units from which the particles are built, and P_0 is a numerical factor depending on their electronic density. Since no Porod region is observed in the patterns (see Figure 3), the size of the elementary building blocks lies outside the measured q range; consequently the value of r_0 has been arbitrarily chosen to be 1 Å during the fitting procedure.

In disordered systems of particles that cannot interpenetrate, the observed peaks are reminiscent of a so-called correlation hole.[25] The simplest model that can mimic this effect and which is applied here is based on a hard sphere interaction between particles. Such a system is characterized by two parameters: the hard sphere volume fraction, ϕ, and the hard sphere interaction distance, R_{hs}. Its structure factor, $S(q)$, is given by[27]

$$S(q) = 1/[1 + 24\phi G(qR_{hs},\phi)/(2qR_{hs})] \tag{8}$$

where G is the following trigonometric function of $x = 2qR_{hs}$ and ϕ:

$$G(x,\phi) = [\sin(x) - x\cos(x)]\frac{\alpha}{x^2} + [2x\sin(x) + (2-x^2)\cos(x) - 2]\frac{\beta}{x^3} + [4[(2x^2-6)\cos(x) + (x^3-6x)\sin(x) + 6] - x^4\cos(x)]\frac{\gamma}{x^5} \tag{9}$$

and α, β, and γ are given by

$$\alpha = (1+2\phi)^2/(1-\phi)^4$$
$$\beta = -6\phi(1+\phi/2)^2/(1-\phi)^4$$
$$\gamma = (\phi/2)(1+2\phi)^2/(1-\phi)^4 \tag{10}$$

Hard sphere effects are expected to be significant if the system is concentrated enough for the mean interparticle distance to be comparable with R_{hs}. The volume fraction ϕ occupied by the hard spheres that is relevant for the structure factor need therefore not be similar to the volume fraction actually occupied by the particles.

The theoretical function eq 6, together with eq 7 and eq 8 for the form and structure factors, is fitted to the time-resolved SAXS patterns by optimization of the five parameters P_0, ξ, D, R_{hs}, and ϕ in a nonlinear least-squares minimization procedure. Figure 5 compares, with linear scales, the measured scattered intensity to the theoretical function, fitted in the q interval between the local minimum of $I(q)$ near $q = 0.01$ Å^{-1} and $q = 0.15$ Å^{-1}, at two different reaction times. The early time corresponds to the onset of the rapid decrease in the position of the peak (see Figure 4b). For ET025, ET04, and ET06, this corresponds to $t = 30$ min, whereas for ET2 $t = 90$ min. The late time corresponds to the end of the runs.

TABLE 1: Morphological Characteristics of the Samples, as Determined from TEM Observations of the Dry Gels and from SAXS Measurements on the Wet Gels[a]

	R_p (Å)	R_a (Å)	R_{hs} (Å)	ϕ	ξ (Å)	l_C^i (Å)	l_C^e (Å)
ET025	115 ± 8	250 ± 17	153 (72)	0.11 (0.03)	46 (15)	229	470
ET04	91 ± 4	198 ± 9	151 (105)	0.12 (0.10)	44 (10)	226	426
ET06	80 ± 8	198 ± 11	150 (109)	0.12 (0.10)	44 (15)	203	426
ET2	49 ± 3	*b*	144 (101)	0.11 (0.10)	38 (6.9)	126	398

[a] R_p, radius of the silica nanoparticles estimated from TEM measurements in ref 20; R_a, radius of the nanoparticle aggregates estimated by TEM and image analysis in ref 21; R_{hs}, ϕ, ξ, hard sphere interaction radius, volume fraction occupied by the hard spheres, and correlation length of the particles estimated by the fitting procedure at the end of the reaction (numbers in parentheses refer to the gel at the onset of phase coarsening); l_C^i, characteristic length of the initial phase-separated domains, estimated from the position of the peak of the exponential growth rate; l_C^e, characteristic length of the final gel estimated from the position of the peak in the SAXS curves at the end of the reaction. [b] Data not available.

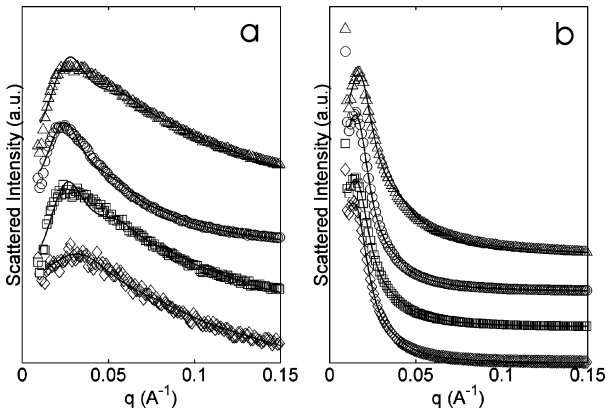

Figure 5. Comparison of measured and fitted scattered intensity profiles for samples ET025 (◇), ET04 (□), ET06 (○), and ET2 (△). (a) and (b) correspond to the gelling solutions at the onset of phase coarsening and to the final gels, respectively. The curves are arbitrarily shifted vertically, and only one point out of three is represented.

The q interval used for the fit had to be limited because (i) the patterns do not follow a power law behavior at very high values of q (Figure 3) and (ii) the SAXS patterns increase at smaller q (Figure 2), which probably reflects a further clustering of the particles at a larger scale[25] that is not accounted for by the model. For low q, i.e., in the region of the peak, the fitting is not satisfactory for small reaction times (Figure 5a) but the quality of the fits globally increases with reaction time. The numerical values of the parameters optimized for both intermediate and final reaction times are reported in Table 1.

3.2. SAXS Comparison of Wet and Dry Gels. SAXS is among the very few experimental techniques than can be applied to characterize both wet and dry solids.[28] To develop an analysis of the wet-sample SAXS patterns that is compatible with what is known about the dry gels, SAXS measurements had to be performed on the dry samples as well.

Figure 6 compares on logarithmic plots the SAXS patterns of the dry gels to the final ones of the wet gels. In the case of ET025, ET04, and ET06 the curves are the same as plotted in Figure 3 at the largest time, i.e., the approximately 2-hour-old wet gels. In the case of ET2, the evolution of the gel is not finished after 2 h, and the pattern of the 6-hour-old gel is used instead, as discussed previously.

The power law exponent of the asymptotic high-q range changes from ca. −2.5 for the wet gels to −4 after drying, and the peak is no longer clearly present in the dry gel patterns. However, in the case of the two samples with the lowest EDAS amounts (ET025 and ET04), a hump is still visible which could be a remnant of the peak. For the sample with the highest amount of EDAS (Figure 6d), the low-q and high-q parts of the dry pattern clearly exhibit two power laws with different exponents.

The dotted lines in Figure 6 are the theoretical SAXS patterns that would be observed from a dilute suspension of monodisperse spherical nanoparticles with the same size as observed in the TEM micrographs. They are calculated as[23−25]

$$I(q) = \left(\frac{\sin(qR_p) - qR_p\cos(qR_p)}{(qR_p)^3}\right)^2 \qquad (11)$$

where R_p is the TEM-based radius[20] as reported in Table 1. At high q, the envelope of the theoretical SAXS patterns obeys a power law with exponent −4, and a plateau is reached below a critical value q_c corresponding to the size of the particles. The oscillations at high q are due to the use of a single nanoparticle radius. They would disappear if a size distribution were introduced. In the case of ET025 and ET04, the hump observed on the experimental curves is located at almost q_c. In the case of ET2, the change of exponent in the experimental pattern occurs near q_c.

4. Discussion

The most striking characteristics of the measured SAXS patterns, independently of the amount of EDAS, are the following. (i) The evolution of the structure at the nanometric scale is independent of the gel point; i.e., no particular event is visible in the SAXS patterns at the macroscopic gel point. This was already noticed for other systems undergoing a sol−gel transition.[5,7] (ii) In the high-q regions, the SAXS patterns obey a power law with an exponent increasing continuously with time, until a value between −2 and −3 is reached at the end of the runs. (iii) In the small-q region, a peak develops with reaction time and progressively shifts toward smaller scattering angles. (iv) At the end of the reaction, the SAXS patterns of the wet gels can be satisfactorily fitted by a model of fractal aggregates interacting with a hard sphere potential and whose elementary units are too small to be detected. (v) In the dry samples, an asymptotic Porod regime is observed with exponent −4. The characteristic peak of the wet gels is no longer visible, and a hump is seen whose position corresponds to the size of the silica nanopartices observed by TEM.

4.1. Possibility of Several Mechanisms. The texture of the studied gels could result from a colloidal aggregation process. Indeed, globular objects are present in the TEM micrographs (Figure 1), and a particulate model can also be fitted on the final wet gel SAXS patterns (Figure 5). However, the main features of the measured temporal evolutions can hardly be accounted for by the colloidal aggregation models traditionally used to describe the sol−gel transition.[1] In the ambit of such models, gelation, which is the event with the largest length scale, occurs when the clusters formed by the aggregated building blocks fill space and touch each other.[1,9,29] During this process, the evolution begins at the smallest scales, when two colloidal

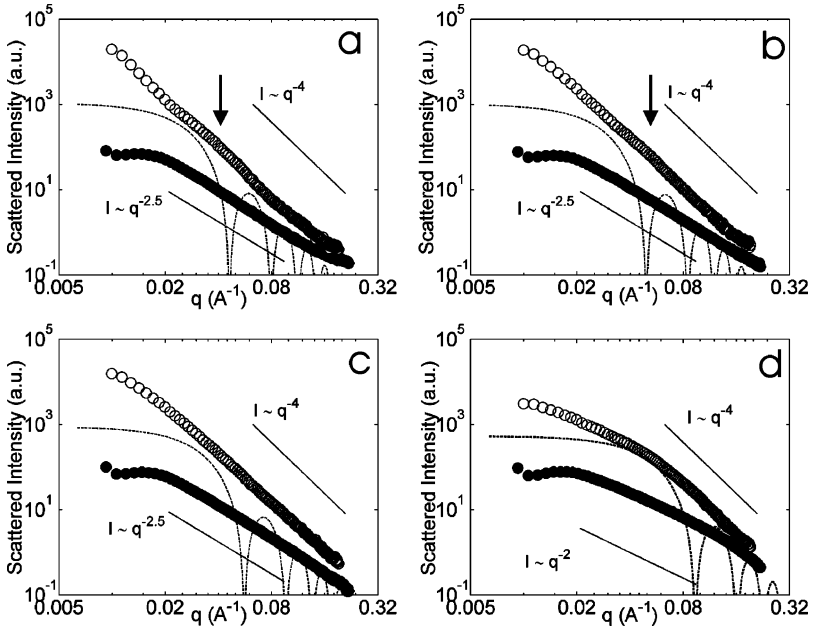

Figure 6. Comparison of SAXS spectra measured on wet (full symbols) and dry gels (open symbols) for samples ET025 (a), ET04 (b), ET06 (c), and ET2 (d). The dotted lines are the theoretical spectra of a dilute suspension of monodisperse spheres whose radius is the same as that of the particles measured on the TEM micrographs.

particles meet, and ends at the largest scales, when the largest aggregates touch each other. What is observed in the present study is the opposite: gelation occurs early, and the nanometric structure continues to evolve until some final state is later reached. Concerning the high-q part of the SAXS patterns, in the case of a pure aggregation, the existence of a unique growth mechanism should lead to an asymptotic power law that keeps the same exponent as the reaction goes on.[4,9,29] It is, however, clear from Figure 4c that the indicative asymptotic exponent increases with reaction time. Such a behavior was observed earlier in aggregating systems[5] and was interpreted as a local smoothing of the structure, resulting from another mechanism that occurs concomitantly but independently of the aggregation itself. These observations show that the gels remain quite mobile at a nanometric scale, even after the macroscopic gel point. Such a contention is indirectly borne by inelastic light scattering measurements[30] that show that tetramethoxysilane-based clusters still possess a significant flexibility very near the gel point.

The most striking characteristic of the low-q part of the SAXS patterns is the presence of a peak. Although the presence of a peak in small-angle scattering curves is not incompatible with the very idea of colloidal aggregation, it usually appears under very specific conditions. It can result either from the regular spacing of monodisperse aggregates as can be obtained from a diffusion-limited aggregation (DLA) mechanism[9] or from the existence of a depletion zone surrounding the growing aggregates.[31] In both cases, the scattering curves recorded at different times can be scaled onto a unique universal master curve, and the position of the peak is thus the only parameter that changes during the material formation. Theoretical arguments exist for such a scaling behavior in the case of cluster−cluster aggregation.[32] In our case, such a scaling is impossible, as can be seen from the change of the asymptotic exponent with reaction time.

When a peak appears in the scattering curves of a multicomponent system, this generally reflects the appearance of a characteristic length scale associated with continuous phase separation. For instance, in the case of spinodal decomposition,[16,33] the existence of a characteristic length results from the competition between the tendency of the polymeric species to cluster and the diffusional limitations that prevent them from separating macroscopically from the solvent. In the case of microphase separation in a cross-linked polymer network,[34] the tendency of like species to cluster is balanced by the polymer entanglement and/or cross-linking. A phase separation model has already been proposed[11,12] to explain the SAXS curves obtained on resorcinol/formaldehyde gels. Given the discrepancies between our time-resolved measurements and the predictions of the colloidal aggregation models, and given the similarities to the data reported for resorcinol/formaldehyde, we explore the possibility of phase separation being responsible for the formation of the wet gels.

4.2. Phase Separation Model. At the very beginning of a polymerization-induced phase separation process, the molecules are miscible with the solvent and the solution is homogeneous. The growth of the molecular weight lowers the entropy of mixing of the species by which phase separation is triggered.[13,17] If demixing occurs via a spinodal decomposition (SD) mechanism, any spontaneous statistical density fluctuations are bound to amplify. Initially, the phase domains and concentration gradients have therefore a comparable size, which leads to a wavelike morphology (Figure 7a,b). The scattering pattern reflects the distribution of concentration wavelengths with a periodicity given by $2\pi/q$ and an attendance given by the corresponding scattered intensity. The favored wavelength can be read from the peak in the scattering patterns. Spatial density or concentration fluctuations in single-phase systems are accurately described by Ornstein−Zernike theory[35] and produce a -2 power law in the scattering patterns. It has been argued that such a power law may appear early during SD.[36] In SD any concentration fluctuation tends to increase with the result that neighboring regions get more and more different in terms of concentration of species (Figure 7c). The sharpening of the concentration gradient continues and in the limit gives rise to an ideal two-phase system with sharp phase boundaries and a Porod power law of -4 in the scattering patterns (Figure 7d). The phase structural evolution continues after the appearance of a sharp interface. This can occur either by syneresis (Figure 7e) or by a coarsening process by which large domains grow at

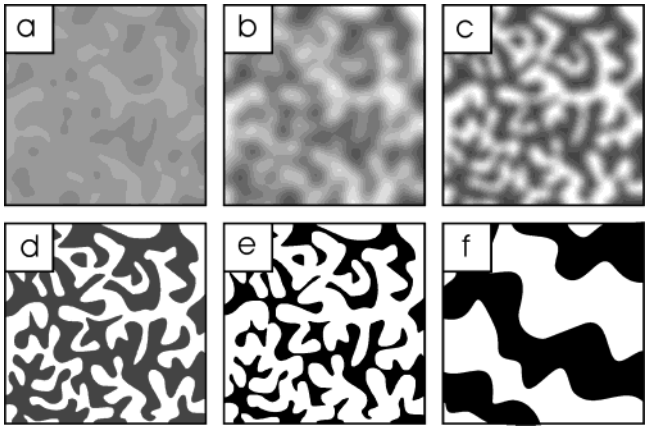

Figure 7. Schematic representation of the three stages of spinodal decomposition: (a) and (b) amplification of the statistical concentration fluctuations during the early stage; (c), (d), and (e) phase differentiation during the intermediate stage; and (f) phase coarsening during the late stage. The degree of darkness represents the density of the polymer-rich phase.

the expense of smaller ones (Figure 7f). This latter evolution is reflected in a shift of the scattering peak toward smaller angles.

This sequence of events, characteristic of SD, can be followed in the EDAS−TEOS systems by considering the evolution of the invariant Q, as is often done for other polymeric systems.[17,18] Let the two phases be a polymer-rich phase (A) with electron density ρ_A, which will eventually contain the percolating network, and an ethanol-rich phase (B) with electron density ρ_B, doomed to become the porosity of the final gel. In the case where the two phases are separated by a linear electron density gradient with thickness E, theoretical calculations show that the invariant can be written as[37]

$$Q = C[\Phi(1 - \Phi) - EO_S/6](\rho_A - \rho_B)^2 \qquad (12)$$

where C is a constant, Φ is the volumic fraction of phase B, and O_S is the specific area of the interface. The precise spatial arrangement of the phases has no influence on the value of Q. The expected evolution of the various terms in eq 12 during the three stages of SD is the following. (i) The factor $(\rho_A - \rho_B)^2$ is expected to increase continuously during early and intermediate stages as the phases become more and more dissimilar. (ii) Since the concentration fluctuations in which the spinodal decomposition originates are described by symmetric sinusoidal waves (see Figure 7a), the corresponding volume fractions of the phases, Φ and $(1 - \Phi)$ are equal to 0.5 during the early stage. Hence, the factor $\Phi(1 - \Phi)$ is maximal at the onset of phase separation, and phase differentiation can only lead to a decrease of this factor (see Figure 7c−e). (iii) During the intermediate stage E decreases with time and the surface tension associated with the interface will drive a decrease of O_S (see Figure 7f). This latter coarsening process is the only one that continues during the *late stage*. If E has reduced to zero by that time, coarsening will not affect Q as the term that contains O_S will have vanished. Otherwise, a reduction of O_S with time will result in an increase of Q. In summary, all quantities in Q tend to an increase except for the factor $\Phi(1 - \Phi)$.

Q is calculated from the scattering data using eq 5 and is plotted in Figure 4a. A maximum is observed in Q, in particular for samples ET04 and ET06. It indicates that Φ shifts away from 0.5 and that beyond the maximum phase separation has evolved into the intermediate stage. For ET025 and ET2 no such maximum is observed, indicating either that, for thermodynamic reasons, Φ is not driven away from 0.5 or that, for kinetic reasons, the intermediate stage of phase separation is not reached. To decide between these two options, it is of interest to look at the evolution of the maximum in the scattering patterns. The position of the peak in the scattered intensity, q_{max}, is associated with a characteristic length of the phase-separated domains through the approximate relation $l_C = 2\pi/q_{max}$. Theory predicts that in the early stage l_C stays constant.[16] In Figure 4b indeed there are clear time lapses with a constant l_C for ET06 and ET2. For the other two samples such a regime is less obvious, pointing to a fast crossover to the intermediate stage. Hence, the absence of a maximum in Q for ET2 may be linked to the retarded transition to the intermediate stage whereas for ET025 Φ seems to remain close to 0.5 during all stages. A Φ value close to 0.5 implies poor phase differentiation and hence a rather small concentration difference between the two phases. The polymer-rich phase in that case contains a substantial amount of ethanol and results in a low $(\rho_A - \rho_B)^2$ factor. It seems therefore from comparison of Q that with increasing amount of EDAS the amount of ethanol in the polymer-rich phase progressively decreases (see Figure 4a). In other words, the EDAS-containing polymers are less miscible with the solvent.

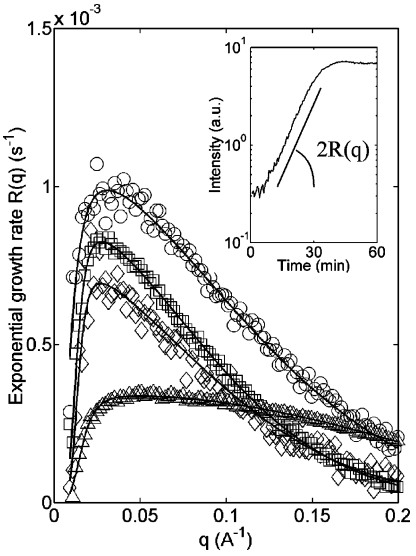

Figure 8. Cahn−Hilliard exponential growth rate for samples ET025 (◇), ET04 (□), ET06 (○), and ET2 (△). The inset shows how $R(q)$ is obtained for ET06 at $q = 0.05$ Å^{-1}.

More evidence for a spinodal type of phase separation can be found in the compatibility of the Cahn−Hilliard theory[16] with the SAXS data during the early stage. According to this theory, the intensity $I(q,t)$ at a given q grows exponentially with time as

$$I(q,t) = I(q,0)\exp(2R(q)t) \qquad (13)$$

where $R(q)$ is an exponential growth rate. An example of semilogarithmic plot of scattered intensity vs time (sample ET06, $q \approx 0.05$ Å^{-1}) is plotted as an inset to Figure 8. Shortly after the beginning of the reaction, a regime where $\ln(I)$ grows linearly with time is observed, which allows $R(q)$ to be calculated. The time range during which the exponential growth is observed for all scattering angles does not last longer than 10 min, except for ET2 where it lasts 20 min. Figure 8 displays the estimated growth rate, $R(q)$, as a function of q for all samples. These curves exhibit a maximum, whose q-position is related to the size of the polymer density fluctuations that are the most unstable, and which determines the length scale of the initial

separated phases (see Figure 7a,b). The position of the peak is converted to the *initial* characteristic length of the domains l_C^i through the relation $l_C^i = 2\pi/q$ and is reported in Table 1 for all samples. These values show that both the interpenetrated solvent- and polymer-rich initial domains become thinner when a larger amount of EDAS is used.

The progressive shift of the peaks toward smaller angles as seen in Figure 4b is characteristic for the intermediate and late stages of SD and reflects phase coarsening. Pure late-stage behavior (constant Q and increase of l_C) can be identified only for ET025; for the other samples Q and l_C seem to evolve at the same time. Several physical mechanisms may be responsible for the coarsening. It is customary to distinguish between hydrodynamic and diffusive coarsening of phase-separated domains.[38] In the case of a diffusion-controlled growth mechanism, such as the sticking or coalescence of initially distinct domains, one would have $l_C \sim t^{1/3}$. In a hydrodynamically controlled mechanism, driven for instance by surface tensions between the two phases, the coarsening should obey $l_C \sim t$. From Figure 4b, one sees that the coarsening seems to be limited more by the hydrodynamics than by diffusional phenomena, which can be taken as argument in favor of the demixing mechanism above the aggregation model. During the same time, the curing reactions continue in the polymer-rich phase, rendering it more and more viscous and/or elastic, and coarsening eventually stops. This is not related to gelation as this happened much earlier. A percolating giant molecule appears in the polymer-rich phase at some intermediate time between the onset of phase separation and the vitrification. This event corresponds to the macroscopic gel point but not to any particular event in the SAXS measurements (see Figure 2).

Since the polymerization goes on continuously from the onset of phase separation until the end of coarsening, it might be argued that the early structures can be locally frozen. We therefore expect that objects with sizes l_C^i can still be present in the gel, even after the phase coarsening. This might be the origin of the particle-like nanostructures visible in Figure 1. The size of these structures measured on the dry gels from TEM micrographs, R_p, decreases when a larger amount of EDAS is used. The initial characteristic length l_C^i follows the same trend (Table 1). On the contrary, the final characteristic length l_C^e is equal for samples ET04 and ET06, which suggests that it is related to the size of the aggregates, R_a (Table 1). These two observations suggest that the globular appearance of the polymer-rich phase is a remnant of the initial phase-separated structure, whereas the size of the aggregates results from the phase coarsening.

Given the compatibility of the SAXS data with theory on SD, it is not surprising that the fitting with a particulate-like morphology does not work in the early stage of demixing. On the other hand, coarsening seems to drive the phase-separated system toward such a structure, as this fitting becomes more and more accurate with time according to Figure 5. Furthermore, the fitted volume fraction occupied by the hard spheres is close to $\Phi = 0.11$ for all samples (Table 1). Considering a sphere touched by p other identical spheres, it is easy to show that the fraction of their spherical envelope occupied by the $(p + 1)$ spheres is $(p + 1)/27$. This expression can serve as an approximate relation between the compactness Φ and the number of neighbors in a packing of hard spheres. Using this expression, the particular value of $\Phi = 0.11$ is found to be equivalent to $p = 2$, which corresponds to a string-of-pearl morphology of the aggregates. This kind of structure is still present in the dry gels (Figure 1) and is also observed in resorcinol/formaldehyde gels.[11,12] Furthermore, recently the occurrence of spinodal decomposition in gels has been shown theoretically[39] to yield to a structure of the polymer-rich phase that is reminiscent of Figure 1.

The question arises about the chemical mechanism by which EDAS has such an influence on the size of the initial phase-separated domains. Due to the presence on it of methyl groups instead of ethyl groups, EDAS is more rapidly hydrolyzed than TEOS. It might therefore be argued that the overall polymerization rate is increased when a larger amount of EDAS is used. In the ambit of chemically induced phase separation, polymerization plays the role of a chemical quench.[13,17] Following this line of reasoning, it is therefore likely that an increase in the EDAS concentration lowers the size of the domains. However, the sample ET2, synthesized with the largest amount of EDAS, seems to behave differently. In particular the growth rate of the most unstable fluctuation (Figure 8) increases continuously from ET025 to ET06 but then suddenly drops for ET2. This trend reversal can be due to two opposing effects produced by an increase of the mean molecular weight. On one hand, it lowers the solubility of the polymeric species, which favors the phase separation, but on the other hand it reduces their mobility. When passing from ET025 to ET06, the increased polymerization rate speeds up the phase separation, but when the EDAS amount is further raised, the dominating effect becomes the loss of mobility so that phase separation (Figures 8 and 4a) and coarsening (Figure 4b) are hindered.

4.3. Drying of the Gels. The SAXS measurements performed on the dry materials aim at determining whether the texture of the dry materials, as estimated by TEM (Figure 1), is representative of the final wet gel whose formation is the main subject of this study.

In contrast to the peak in the wet gel SAXS patterns, a faint hump is observed in the dry SAXS patterns superimposed on a globally decreasing intensity with -4 exponent (Figure 6). This Porod-like behavior can be due to the scattering by large pores that overwhelms the scattering by the gel internal structures. This explanation is confirmed by mercury porosimetry and nitrogen adsorption measurements that show that the dry gels are highly meso- and macroporous.[20,21] Furthermore, Figure 1 shows that the spinodal-like structures described in Figure 7 are still present in the dry gels, at a length scale that should make them visible by SAXS. The relevance of the hump is further confirmed by the fact that its q-position coincides with the size of the globular silica structures measured by TEM. The position of the hump is shifted toward smaller scales, compared to the peak. This shrinking is not surprising and has to be related to compaction of the structures during the drying stage. This compaction is also responsible for the evolution of the asymptotic slopes from ca. -2.5 to -4 during drying. This reflects the transition from structures with diffuse interfaces to a material with clearly defined interfaces.

One of the desirable characteristics of the studied gels is that they keep a large porosity even when dried in subcritical conditions. During drying, a gel shrinks because of the collapse of those structures whose mechanical strength is lower than the stress caused by the capillary forces. The two factors affecting the shrinking of the material during drying are therefore the capillary stresses and the mechanical strength of the material. It has been previously argued[20] that the relatively large pore size in EDAS/TEOS gels is responsible for the large porosity of the dry gels, due to a reduction of the capillary pressure. An additional argument is the following. In materials with a broad pore size distribution, the larger pores contribute generally to a

large amount of the overall porosity. These larger pores are also the most fragile and are likely to collapse during drying.[40] Compared to fractal-like structures resulting from, e.g., the diffusion-limited aggregation of colloidal particles, the structures resulting from phase separation have a narrow pore size distribution, which is reflected in their having a characteristic length. The shrinking of the material through the collapse of larger pores is therefore avoided. One can thus argue that the very mechanism of phase separation can contribute to the EDAS/TEOS gels' ability to preserve a large porosity during drying.

5. Conclusions

Time-resolved SAXS measurements were performed on a series of silica gels synthesized with an additive. A comparison of the measured data with previous studies concerning other porous materials reveals that a phase separation mechanism is responsible for the nanometric structure of the final dry gel. This conclusion is supported by the presence of a peak in the SAXS patterns of these materials and by the observation that no discontinuity in the nanostructural evolution occurs at the macroscopic gel point. Moreover, the model developed for the wet gel formation allows for an original interpretation of the SAXS patterns associated with the dry gels.

In the ambit of the proposed spinodal decomposition model, physical reasons are proposed for the observed influence of the amount of the specific additive on the nanometric structure of the wet gel. The EDAS concentration is shown to control the scale at which the phases initially separate. It is suggested that the particle-like objects visible in the dry gels are remnants of the early phase-separated domains, and that the phase coarsening controls the size of the aggregates.

Should the proposed physical mechanisms be further confirmed, their deep understanding and control would certainly open new ways in which the texture of these materials could be tailored to better fit a precise application.

Acknowledgment. C.G. and C.A. are grateful to the FNRS (National Fund for Scientific Research, Belgium) for a Ph.D. Research Fellow and a Postdoctoral Researcher positions. B.G. is a postdoctoral fellow of the Fund for Scientific Research Flanders (FWO-Vlaanderen). The authors thank Wim Bras and Igor Dolbnya (DUBBLE-CRG/ESRF) for their assistance in acquiring the in situ SAXS patterns, and Monika Basiura (Catholic University of Leuven) for acquiring the SAXS patterns on the dry gels. The authors thank H. Reynaers (Catholic University of Leuven) and the FWO-Vlaanderen for support of the DUBBLE project. This work was supported by the Action de Recherche Concertée 00/05-265 of the Communauté Française de Belgique.

References and Notes

(1) Brinker, C. J.; Scherer, G. W. *Sol-Gel Science: The Physics and Chemistry of Sol−Gel Processing*; Academic Press: San Diego, 1990.
(2) Schmidt, M.; Schwertfeger, F. *J. Non-Cryst. Solids* **1998**, *225*, 364.
(3) Hrubesh, L. W. *J. Non-Cryst. Solids* **1998**, *225*, 335.
(4) Schaefer, D. W.; Keefer, K. D. *Phys. Rev. Lett.* **1984**, *53*, 1383.
(5) Blanco, E.; Ramirez-del-Solar, M.; de la Rosa-Fox, N.; Craievich, A. F. *J. Non-Cryst. Solids* **1992**, *147&148*, 238.
(6) Vollet, D. R.; Donatti, D. A.; Ibanez Ruiz, A. *J. Non-Cryst. Solids* **2001**, *288*, 81.
(7) Lebon, S.; Marignan, J.; Appel, J. *J. Non-Cryst. Solids* **1992**, *147&148*, 92.
(8) Chaumont, D.; Craievich, A.; Zarzycki, J. *J. Non-Cryst. Solids* **1992**, *147&148*, 127.
(9) Lecomte, A.; Dauger, A.; Lenormand, P. *J. Appl. Crystallogr.* **2000**, *33*, 496.
(10) Schmidt, P. W. *J. Appl. Crystallogr.* **1991**, *24*, 414.
(11) Pekala, R. W.; Schaefer, D. W. *Macromolecules* **1993**, *26*, 5487.
(12) Schaefer, D. W.; Pekala, R.; Beaucage, G. *J. Non-Cryst. Solids* **1995**, *186*, 159.
(13) Kaji, H.; Nakanishi, K.; Soga, N.; Inoue, T.; Nemoto, N. *J. Sol-Gel Sci. Technol.* **1994**, *3*, 169.
(14) Flory, P. *Principles of Polymer Chemistry*; Cornell University Press: Ithaca, NY, 1971.
(15) de Gennes, P.-G. *Scaling Concepts in Polymer Physics*; Cornell University Press: Ithaca, NY, London, 1979.
(16) Olabisi, O.; Robeson, L. M.; Shaw, M. T. *Polymer-Polymer Miscibility*; Academic Press: New York, 1979.
(17) Ishii, Y.; Ryan, A. J. *Macromolecules* **2000**, *33*, 158.
(18) Elwell, M. J.; Ryan, A. J.; Grünbauer, H. J. M.; Van Lieshout, H. C. *Macromolecules* **1996**, *29*, 2960.
(19) Heinrichs, B.; Delhez, P.; Schoebrechts, J.-P.; Pirard, J.-P. *J. Catal.* **1997**, *172*, 322.
(20) Alié, C.; Pirard, R.; Lecloux, A.; Pirard, J.-P. *J. Non-Cryst. Solids* **1999**, *246*, 216.
(21) Blacher, S.; Alié, C.; Gommes, C.; Lodewyckx, P.; Pirard, R.; Pirard, J.-P. *Stud. Surf. Sci. Catal.* **2002**, *144*, 323.
(22) Lenza, R. F. S.; Vasconcelos, W. L. *J. Non-Cryst. Solids* **2003**, *330*, 216.
(23) Glatter, O.; Kratky, O. *Small-angle X-ray Scattering*; Academic Press: New York, 1982.
(24) Schmidt, P. W. Some Fundamental Concepts and Techniques Useful in Small-Angle Scattering Studies of Disordered Solids. In *Modern Aspects of Small Angle Scattering*; Brumberger, H., Ed.; Kluwer Academic Publishers: Dordrecht, 1995; p 1.
(25) Mortensen, K. Structural studies of polymer systems using small-angle neutron scattering. In *Advanced Functional Molecules and polymers*; Nalwa, H. S., Ed.; Overseas Publishers Association: Amsterdam, 2001; p 223.
(26) Teixeira, J. *J. Appl. Crystallogr.* **1988**, *21*, 781.
(27) Mortensen, K.; Pedersen, J. K. *Macromolecules* **1993**, *26*, 805.
(28) Kaneko, K. *J. Membr. Sci.* **1994**, *96*, 59.
(29) Dietler, G.; Aubert, C.; Cannel, D. S.; Wiltzius, P. *Phys. Rev. Lett.* **1986**, *57*, 3117.
(30) Martin, J. E.; Keefer, K. D. *Phys. Rev. A* **1986**, *34*, 4988.
(31) Carpineti, M.; Giglio M.; Degiorgio, V. *Phys. Rev. E* **1995**, *51*, 590.
(32) Hasmy, A.; Jullien, R. *J. Non-Cryst. Solids* **1995**, *186*, 342.
(33) Guenoun, P.; Gastaud, R.; Perrot, F.; Beysens, D. *Phys. Rev. A* **1987**, *36*, 4876.
(34) de Gennes, P.-G. *J. Phys. Lett.* **1979**, *40*, 69.
(35) Stanley, H. E. *Introduction to phase transitions and critical phenomena*; Clarendon Press: Oxford, 1971.
(36) Schaefer, D. W.; Bunker, B. C.; Wilcoxon, J. P. *Proc. R. Soc. London, A* **1989**, *423*, 35.
(37) Vonk, C. G. *J. Appl. Crystallogr.* **1973**, *6*, 81.
(38) Siggia, E. D. *Phys. Rev. A* **1979**, *20*, 595.
(39) Onuki, A.; Puri, S. *Phys. Rev. E* **1999**, *59*, 1331.
(40) Ma, H. S.; Roberts, A. P.; Prévost, J. H.; Jullien, R.; Scherer, G. W. *J. Non-Cryst. Solids* **2000**, *277*, 127.